

Supporting Information:

LK peptide side chain dynamics at interfaces are independent of secondary structure

*Michael A. Donovan,^a Helmut Lutz,^a Yeneneh Y. Yimer,^b Jim Pfaendtner,^b Mischa Bonn^a and
Tobias Weidner^{*a,b,c}*

AUTHOR ADDRESS

^aMax Planck Institute for Polymer Research, Ackermannweg 10, 55128 Mainz, Germany

^bDepartment of Chemical Engineering, University of Washington, Seattle, WA 98195, United States

^cDepartment of Chemistry, Aarhus University, Langelandsgade 140, 8000 Aarhus C, Denmark

Table of Contents

I.	Experimental Section	2
II.	Single-exponential fits to transients, vibrational lifetime	3
III.	Anisotropy decay	6
IV.	Vibrational relaxation within orientation model	8
V.	Molecular Dynamics Simulations	9
VI.	Analysis of MD results	11
VII.	Hydrogen bonding might affect side chain methyl IVR	14
VIII.	Numerical simulation of transient orientation dependent SFG signal	14
IX.	References	15

I. Experimental Section

Briefly, 2 mJ of the output from a 5 mJ, 1 kHz regenerative Ti:Sa amplifier (Spectra Physics Spitfire Pro) is divided evenly between two commercial optical parametric amplifiers (TOPAS, Light Conversion) the first of which generates broadband ($\sim 400\text{ cm}^{-1}$) mid IR inside of an internal AgGaS₂ DFG crystal. Additionally for the probe, 1.5 mJ of broadband 800 nm light is frequency narrowed by a Fabry Perot etalon to produce $\sim 15\text{ cm}^{-1}$ bandwidth pulses for the VIS beam. The idler wave from the second TOPAS is frequency doubled and mixed with 0.5 mJ from the fundamental 800 nm beam inside of a KTP crystal and intense mid IR pulses ($\sim 100\text{ }\mu\text{J}$) are generated via optical parametric amplification and difference frequency mixing.¹ The pump beam is then passed through a computerized delay stage (Physik Instrument) before being mechanically chopped (Thor Labs) at 500 Hz. Planoconvex CaF₂ lenses of $f = +5\text{ cm}$ and $f = +15\text{ cm}$ are used to focus the IR pump and probe into the sample plane, while an AR coated planoconvex $f = +20\text{ cm}$ lens is used to focus the 800 nm beam. Spectra are acquired by first separating the pump-on to pump-off spectra via displacement by a galvano mirror triggered by the laser vibrating at 500 Hz. Signals are subsequently dispersed in an Acton Spectrometer (blaze 600 nm 1200 g/mm) and dispersed onto a peltier cooled EM CCD detector (Newton Andor). Labview software is used to control the delay stage and acquire the spectra. Bulk solutions of LK peptide (LK α 14: Ac-LKKLLKLLKLLKL-OH, LK β 15: Ac-LKLLKLLKLLKLLKL-OH, LK₃₁₀: Ac-LLKLLKLLKLLKL-OH) of 0.1 mg/mL in D₂O were used. D₂O was used instead of H₂O to reduce laser heating to the subphase and to avoid interference with the underlying band of the OH stretching vibration with the aliphatic stretching region. Solutions were poured into a Teflon trough which rotates

at ~ 7 rpm to reduce laser heating from the mid IR pump pulse. The water level was replenished continuously to account for any evaporation that occurs during the measurement cycle. Angles of incidence for the mid IR pump, mid IR probe, and 800 nm beam are respectively 57° , 46° , and 54° from the surface normal. Beam energies for IR pump, IR probe and VIS respectively are $20\mu\text{J}$, $3\mu\text{J}$, and $4.5\ \mu\text{J}$. The data presented for the 3_{10} and β peptides are the average of the ratio of pump on to pump off SFG spectra of 28 and 33 scans acquired under EM amplification at an acquisition time of 45s per spectrum for 3_{10} and β peptides respectively; α peptides were acquired under EM for 75s per spectrum with a total of 12 scans averaged. Static spectra presented in the manuscript are normalized to IR intensity spectrum from the non-resonant SFG response from a z-cut quartz reference. Time traces shown are acquired by integrating over the region from $2945\ \text{cm}^{-1}$ to $2970\ \text{cm}^{-1}$ and subsequently from the pump on to pump off ratio. Instrumental response times are determined from 154 fs Gaussian fits to the Infrared infrared visible correlation function and are convoluted with the numerical model results.

II. Single-exponential fits to transients, vibrational lifetime:

As described in the main text, single exponential fits are performed in Origin Pro 9 software by performing a monoexponential ($y = y_0 + Ae^{-t/\tau}$) fit to the data starting at $t > 250$ fs via a Levenberg Marquardt algorithm for least squares analysis. Before fitting, the experimental data is smoothed with a two point adjacent averaging filter. Data were fit so as to not include the instrumental response function (154 fs Gaussian) into the analysis. By fitting at times 100 fs greater than the instrumental response, the influence of the pulse shape on the signal can be neglected, and the signal should follow the population dynamics. The data might be better visually presented with an iterative re-convolution algorithm, but the standard error in the single exponential lifetimes may in principle be reduced by increasing the number of pump-

probe delay points acquired after the instrumental response. Due to the long signal acquisition times required, this approach sacrifices overall measurement times.

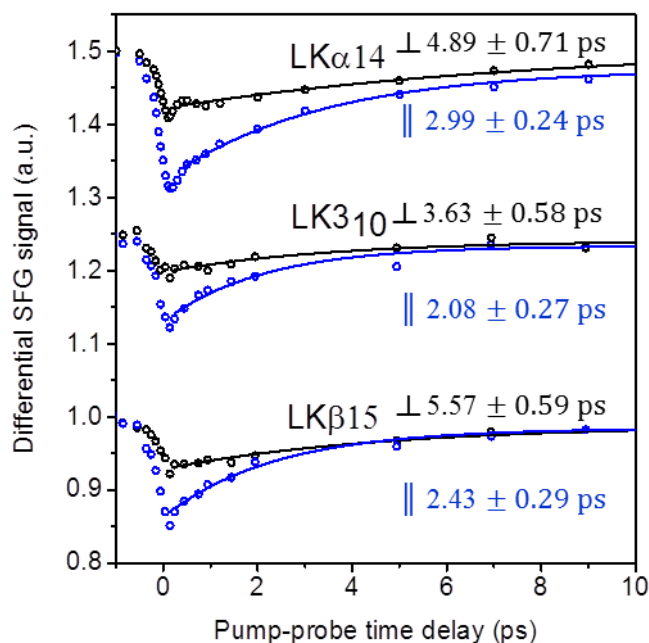


Figure S1 Monoexponential decay fits to transients of LK peptides

From these single exponential fits, we attempt to estimate the orientation times via a simple kinetic model introduced in our previous study on Leucine² which includes overall reorientation and vibrational relaxation.

Based on the fitting results we can approximate the vibrational relaxation times T_1 and the effective reorientation time $T_{\text{eff, reor}}$ from:²

$$k_1 = 1/2(k_{\parallel} + k_{\perp}) = 1/T_1 \quad (s1)$$

$$k_{\perp} = k_1 - k_{\text{eff, reor}} \quad (s2)$$

$$k_{\parallel} = k_1 + k_{\text{eff, reor}} \quad (s3)$$

$$k_{\text{eff, reor}} = 1/2(k_{\parallel} - k_{\perp}) = 1/T_{\text{eff, reor}} \quad (s4)$$

An effective rate of reorientation ($k_{\text{eff, reor}}$) and a vibrational relaxation rate (k_1) can be calculated from equations (s2) and (s3). The experimentally measured parallel (perpendicular) dynamics are sped up (slowed down) due to reorientation by a factor of $k_{\text{eff, reor}}$ as shown in equations s2 - s3. If we then infer that the vibrational relaxation rate k_1 is calculated from the average of the rate constants of the two traces (k_{\parallel} , k_{\perp}) as shown in equation (1), we estimate that for LK α 14, LK β 15, and LK3 $_{10}$, the effective orientational time coefficients $T_{\text{eff, reor}}$ respectively equal 15 ± 8 ps, 9 ± 4 ps and 10 ± 7 ps. While the results are of the same order as $T_{\text{eff, reor}}$ values published for leucine monomers at the air-water interface, the large error margins involved in this analysis make it difficult to draw conclusions about how the side chains' dynamics are affected by the peptide folding. According to eqs s1- s4, we can approximate T_1 as well, and this value is presented in table S1. This vibrational relaxation rate estimated from simple exponential fits to the data and from equations s1 to s4 in the SI follows the same qualitative trend we see from the resultant numerically simulated traces of $k_{310} > k_{\beta} > k_{\alpha}$.

Table S1. Experimentally determined time and rate constants. Error margins are given in parenthesis.

Peptide	$\tau_{1,\parallel}$ ps	$\tau_{1,\perp}$ ps	T_1 ps	τ_{ani} ps	D_{ϕ}^{ani} $\text{rad}^2\text{ps}^{-1}$
LK α 14	2.99 (0.24)	4.89 (0.71)	3.71 (0.28)	2.09 (0.37)	0.13 (0.02)
LK β 15	2.43 (0.29)	5.57 (0.59)	3.38 (0.30)	0.97 (0.11)	0.26 (0.03)
LK3 $_{10}$	2.08 (0.27)	3.63 (0.58)	2.64 (0.26)	1.39 (0.45)	0.18 (0.06)

III. Anisotropy decay:

For the xzx component of the nonlinear susceptibility tensor $\chi^{(2)}$ which is probed the sps polarization combination, the time dependent in plane anisotropy decay $r(t)$ is defined as:³

$$r(t) = c_-/c_+ = \frac{1}{2} e^{-4D_\phi t}$$

$$c_- = \Delta\chi(t)_{xzx:x}^{(2)} - \Delta\chi(t)_{xzx:y}^{(2)}$$

$$c_+ = \Delta\chi(t)_{xzx:x}^{(2)} + \Delta\chi(t)_{xzx:y}^{(2)}$$

$$c_-/c_+ = \frac{I_s - I_p}{I_s + I_p} = \frac{I_{||} - I_{\perp}}{I_{||} + I_{\perp}} =$$

$$r(t) = (I_{||} - I_{\perp}) / (I_{||} + I_{\perp}) = e^{-t/\tau_{ani}} = \frac{1}{2} e^{-4D_\phi t}$$

D_ϕ is the in plane diffusion constant; $\Delta\chi_{ijk}^{(2)}$ are the probed transient second order susceptibility elements; I_i is the measured bleach intensity, and τ_{ani} is the anisotropy decay time constant. Single exponential fits to this anisotropy decay follow a similar procedure to what is described above for the experimental traces. First, the anisotropy decay between the smoothed raw data is calculated, and single exponential fits to this data are performed to extract the rate of anisotropy decay. For $\sin\theta_0 \gg \Delta\theta$, the decay of anisotropy describes the in plane orientational dynamics. In the case of the LK peptides studied, there is likely an effect due to out of plane reorientation which cannot be discounted particularly in the case of LK β , but to a large extent, the decay of the anisotropy in the sps polarization combination should be dominated by in plane reorientation dynamics.³ Other measurement schemes such as that with an excitation pulse circularly polarized and normal to the surface presented in reference³ can measure the c_+ component which should only be affected by out of plane reorientation and vibrational relaxation. We note, however, that this approach is experimentally challenging.

In addition, the sps polarization combination was chosen due to the fact that according to our previous study, the ssp polarization combination is not particularly sensitive to orientational dynamics in the systems (i.e. leucine methyls) studied as indicated by the pump-probe traces.² In addition, the sps polarization combination allows us to monitor the decay in the xzx tensor component's anisotropic signal which is a vast simplification of the ppp polarization scheme's multiple tensor components.

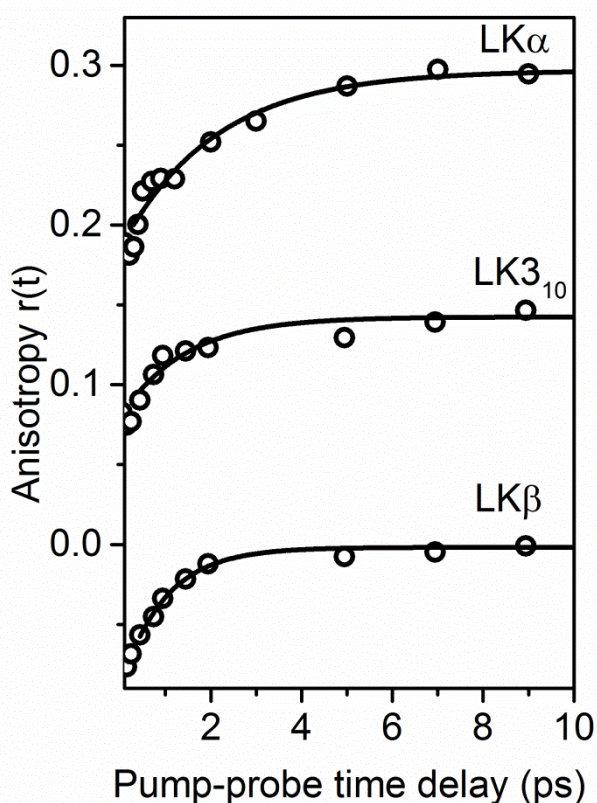


Figure S2 Anisotropy (open circles) and exponential fits (solid lines) for the three folds of LK peptide study. Fitting results are presented in table S1 for τ_{ani}

The anisotropy decay presented in Figure S2 and summarized in table S1 measures the effect that in plane molecular reorientation has on the SFG signal and should inherently exclude out of plane reorientation in limiting cases of small tilt angle spread. By fits to the anisotropy decay for the peptides studied, the diffusivities of $D_{\phi} = 0.13, 0.18,$ and $0.26 \text{ rad}^2/\text{ps}$

are respectively calculated for LK α 14, LK3₁₀, and LK β 15. This is for LK β 15 twice the rate MD suggests, and the rates are comparable to the MD simulation calculated rate values for LK α 14 and LK3₁₀. Since the peptides display a large tilt angular spread $\Delta\theta$, this indicates that $r(t)$ may include contributions from vibrational relaxation and out of plane dynamics.³ Because of the large tilt angle spread, we cannot use the anisotropy decay to make quantitative comparisons about side chain dynamics. Nonetheless, the anisotropy can provide a preliminary estimate of the orientational dynamics before extensive computational modelling.

IV. Vibrational relaxation within orientation model:

In figure S3, the effect of a variable relaxation rate k_1 is shown for the different folds of LK peptide studied. For LK α 14, the best visual match of the simulated data appears when the vibrational relaxation time (rate) is chosen to be approximately 3.3 ps (0.3 ps^{-1}); a T_1 (k_1) value of 2.5 ps (0.4 ps^{-1}) appears to underestimate the recovery of the signal. For LK β 15 and LK3₁₀, the opposite appears to be true. Relaxation times T_1 of 3 ps appear to overestimate the recovery of the dynamics while shorter relaxation times appear to match the signal recovery well. We may also further discuss the T_1 values estimated from equations 1 to 4 in the main text. The trend of vibrational relaxation obtained from equations 1 to 4 in the main text give the same qualitative trend with T_1 being least for LK3₁₀ < LK β 15 < LK α 14, but within the error margins of this calculation, it can only be said that LK3₁₀ displays accelerated vibrational relaxation. We arrive at the conclusion that vibrational energy transfer might be different for the varying folds based on a) the sensitivity of the numerical model to the relaxation times, b) the qualitative difference brought from our equations 1 to 4 in the main text, and c) based on discrepancies in the anisotropy. To investigate what leads to possible differences in IVR, we turned to the MD simulations to investigate possible hydrogen

bonding effects for different folds of peptide. This is briefly discussed in the next subsection detailing molecular dynamics simulations.

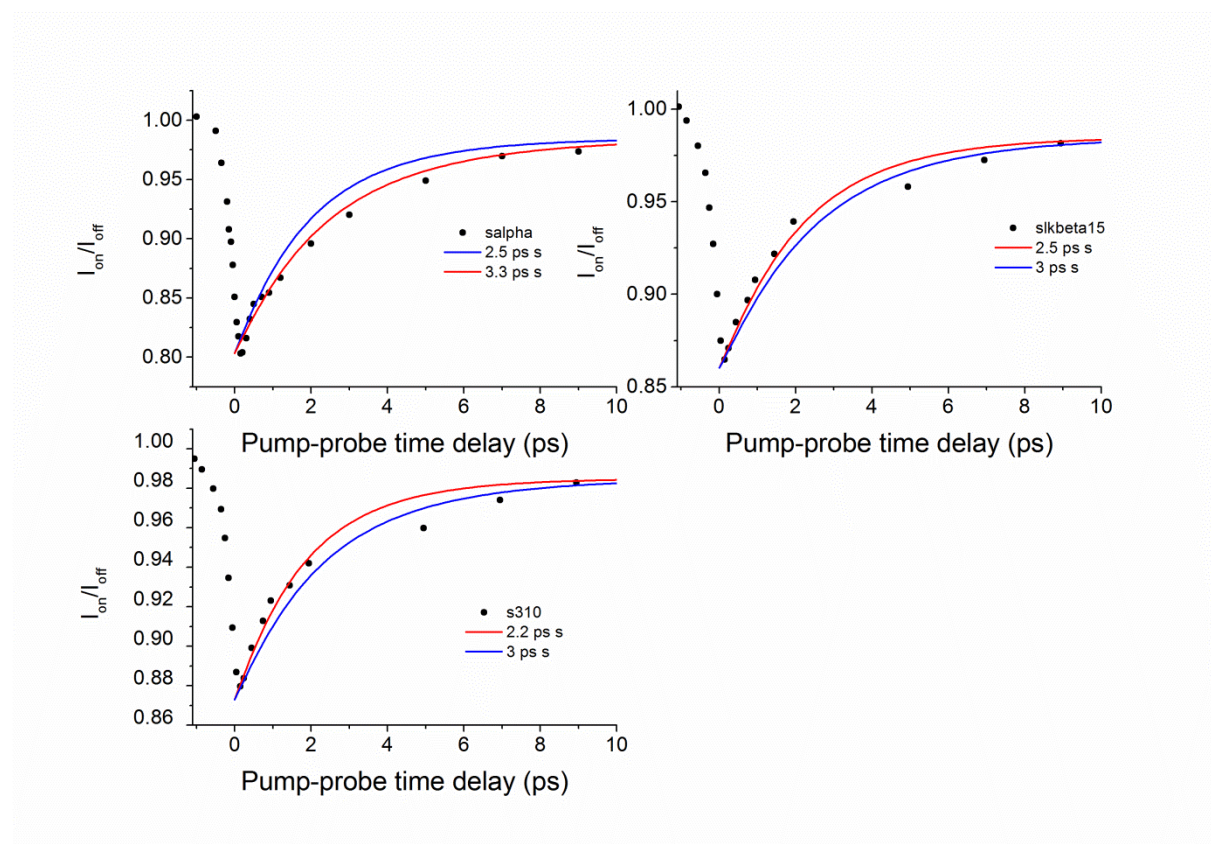


Figure S3 Sensitivity of numerical model to vibrational relaxation for the three LK peptides studied. Top left LK α 14, top right LK β 15, bottom left LK3 $_{10}$. Best visual match shown in red.

V. Molecular Dynamics Simulations

The simulation box was set up using the software Packmol.⁴ 23 peptides were arranged at the surface of a 8 x 8 x 6.8 nm slab of water. The water slab contained 10 phosphate anions and enough chloride anions to neutralize the simulation box. Prior to running the simulation, the simulation box was extended in the z direction by 7 nm such that the peptides resided at the water-vacuum interface. Thus, the peptides were simulated at the surface of 6.8 nm thick slabs of water, which were separated by 7 nm of vacuum. AMBER99SB-ILDN parameters were applied for the peptides.⁵ TIP3P parameters were used for water molecules and

phosphate ion parameters were adapted from ref. ⁶. The software Tleap was used to produce topology and coordinate files. These files were converted to GROMACS-type input files using the software Acpype.^{7, 8} Atomistic molecular dynamics simulations were set up and run using the software package GROMACS 4.6.⁹ All bonds were constrained with the LINCS algorithm. Simulations were run with periodic boundary conditions in the x-, y- and z-dimension at a 2 fs time step for 100 ns. Long-range coulombic interactions were taken into account by the particle mesh Ewald (PME) method.¹⁰ The cut-off distance for the Lennard-Jones potential was set to 1 nm and velocity rescaling with a stochastic term was employed to maintain the temperature of the simulation at 300 K.¹¹ After the initial 100 ns simulation, 5 ns were simulated at a time step of 2 fs where the trajectory was recorded at a 4 fs time step. This time step was necessary for the subsequent extraction of reorientation times.

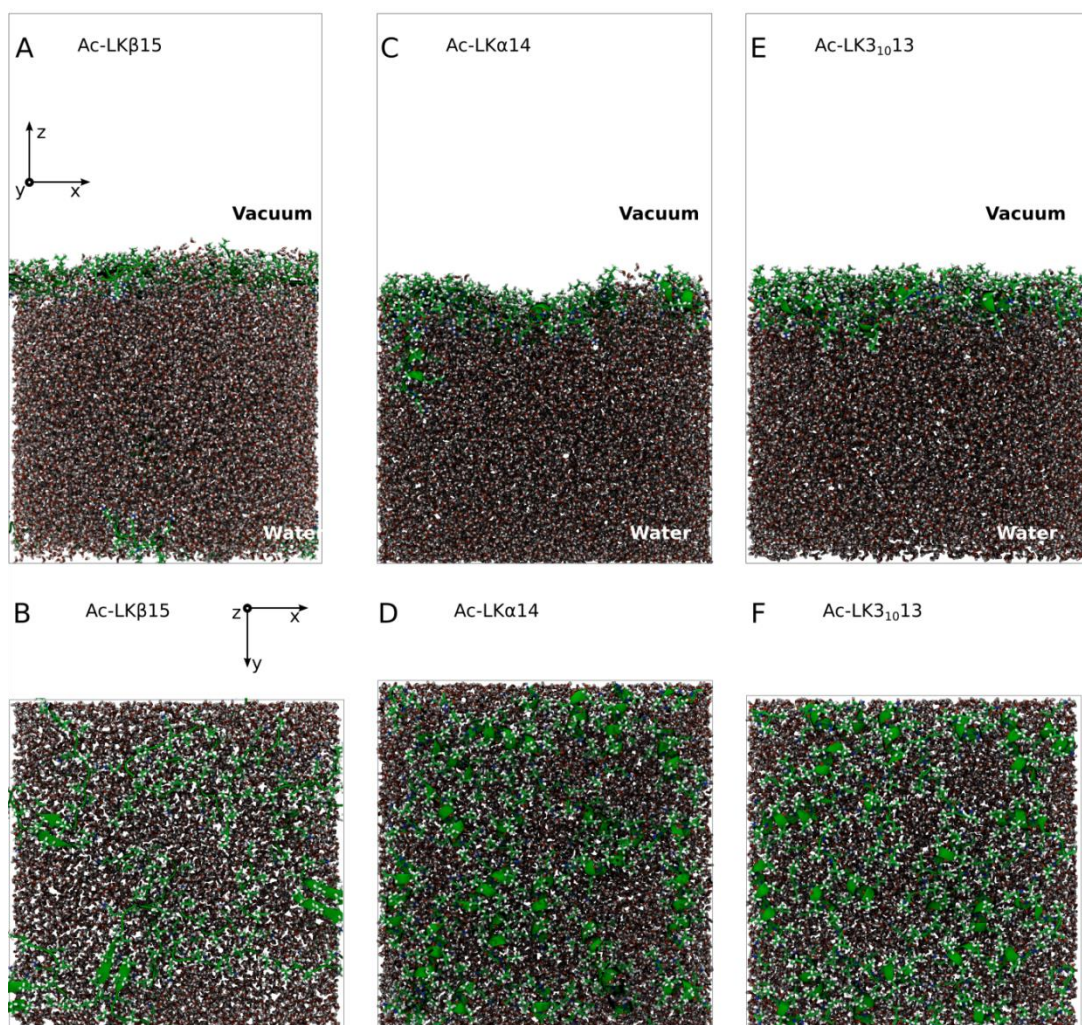


Figure S4 (A-F) Side and top views of the simulations box for the respective 3 LK peptide folds.

VI. Analysis of MD results

MD simulations trajectories were analyzed in a similar manner to a recent publication on Leucine² and analogous to a procedure used by Hsieh et. Al to extract orientational diffusion coefficients for water.¹² The mass density profile of water was calculated by partitioning the simulation box into 1 Å-thick bins along the z -axis and calculating the total mass in each bin per partition volume. A region at which the mass density of water is less than the bulk density (middle region) is defined as an interfacial region. To determine whether a leucine molecule

belongs to the interfacial region or not the position of the C_{α} atom (of leucine side chains) is used as a reference.

As shown in Figure S5 and in the main text, the orientational vector of the methyl group is defined as a unit vector originating from the carbon atom (on the methyl group) and terminating at the geometric center of the three hydrogen atoms (on the methyl group). Angle θ (polar angle) is defined by the angle between the unit vector and the Z-axis (a vector normal to the LK-water slab surface). The angle φ (azimuthal angle) is defined as the angle between the orientational vector projection on the xy-plane and the x-axis. Figure S3 a-c shows the azimuthal φ angle distributions of LK side chain methyl groups at the air-water interface. Azimuthal and tilt angle distributions shown in the SI and the main text are the average distributions of both methyl groups along the different leucine residues.

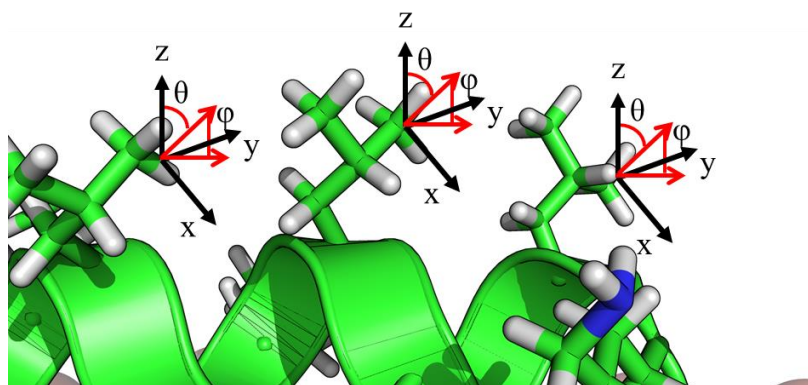


Figure S5 Definition of azimuthal and tilt angle for generalized LK peptide.

Figures S6 a-c show the azimuthal symmetry of the leucine side chain methyls for the different folds of LK peptide at the air/water interface. In equilibrium, the methyls are shown to display no preferential orientation in the surface plane.

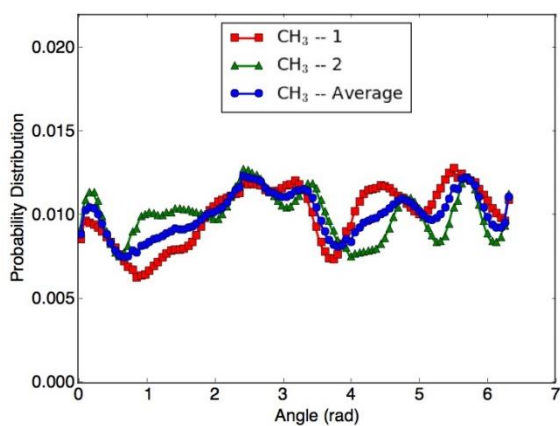


Figure S6 a) Azimuthal ϕ angle distribution for LK α 14 methyls

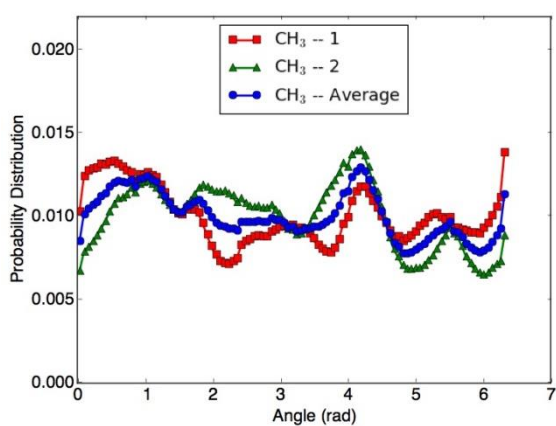


Figure S6 b) Azimuthal ϕ angle distribution for LK β 15 methyls

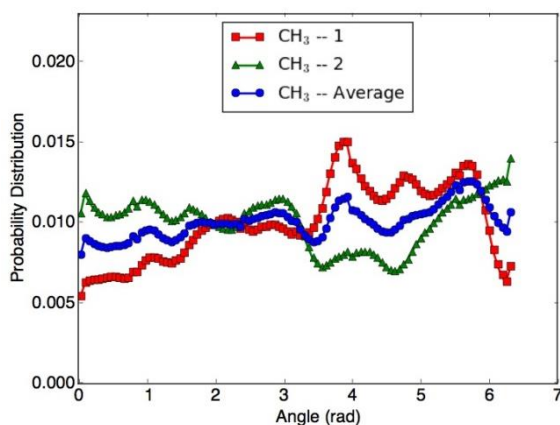


Figure S6 c) Azimuthal ϕ angle distribution for LK3₁₀ methyls

For the methyl group reorientation, diffusion coefficients D_θ (out of the plane of the surface) and D_ϕ (in plane of the surface) were calculated following a similar procedure previously used by Hsieh et al and also used in our previous leucine work.^{2, 12} The molecular dynamics

simulations track the population of methyl groups that at time 0 are within the range of $0 < \varphi < 180$ and $34 < \theta < 96$, and subsequently we observe this population relax towards equilibrium. Using the methyl angle distribution (θ, φ) obtained from the MD simulation as an initial boundary value, a two dimensional diffusion equation (given in Equation 1 of the SI of ref. ¹²) was solved for different guessed values of D_θ and D_φ . Then, we calculated the square of residuals, χ^2 , to determine the goodness of a fit between the angle distributions (θ, φ) obtained from the numerical solution using the diffusion equation and MD simulation results. Values for θ_0 and $\Delta\theta$ are calculated based on simple Gaussian fits to the equilibrium angular distribution extracted from the simulation trajectories. Gaussian fits were chosen as a way to simplify the data analysis.

VII. Hydrogen bonding might affect side chain methyl IVR

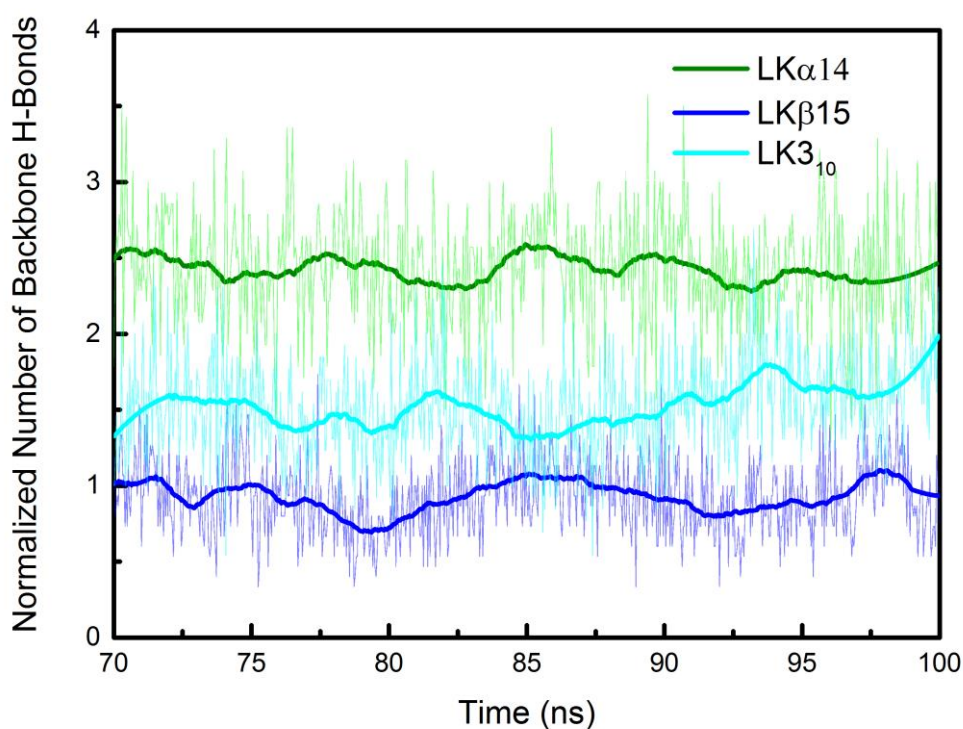


Figure S7 The number of hydrogen bonds were obtained for the last 30 ns of a 100 ns simulation with the HBonds plugin of VMD.¹³ Light colors represent the number of hydrogen

bonds at the respective time point. The data was smoothed by the Savitzky-Golay filter using second order polynomial fitting on windows of 100 data points (thick lines).¹⁴

VIII. Numerical simulation of transient orientation dependent SFG signal

Details of the numerical model used to simulate the SFG signal are thoroughly presented in a previous publication.³ Parameters for the model are as follows. First, the two dimensional diffusion equation in spherical coordinates is numerically solved to find solutions of the angle dependent population distribution ρ for both parallel and perpendicular pump polarization.

$$\frac{\partial \rho}{\partial t} = \frac{D_\varphi}{\sin^2 \theta} \frac{\partial^2 \rho}{\partial \varphi^2} + \frac{D_\theta}{k_B T} \frac{\partial \rho}{\partial \theta} \frac{\partial V}{\partial \theta} + \rho \frac{D_\theta}{k_B T \sin \theta} \frac{\partial}{\partial \theta} \sin \theta \frac{\partial V}{\partial \theta}$$

given a harmonic potential dependent on tilt angle V:

$$V(\theta) = \frac{k_B T}{2(\Delta\theta)^2} (\theta - \theta_0)^2$$

can be related to the transient SFG response by:

$$\Delta\chi^{(2)}(t) = - \iint \rho_\sigma(\varphi, \theta, t) \beta(\theta, \varphi) d\varphi d\theta$$

where $\Delta\chi^{(2)}(t)$ is the transient susceptibility tensor and $\beta(\theta, \varphi)$ is the molecular hyperpolarizability, $k_B T$ is the thermal energy, $\Delta\theta$ is the tilt angle spread, and θ_0 is the mean tilt angle. The temporal evolution of the signal is directly proportional to $\Delta\chi^{(2)}(t)$.

Model parameters are set such at $14.8 = k_B T$. Angular parameters such as $\Delta\theta$ and θ_0 (Table 1 main text) are determined by analyzing the trajectories of the MD simulations as described in the MD simulations section to the SI which is similar to the analysis presented for L-Leucine in reference.²

IX. References

1. U. Emmerichs, S. Woutersen and H. J. Bakker, *J. Opt. Soc. Am. B*, 1997, **14**, 1480-1483.
2. M. A. Donovan, Y. Y. Yimer, J. Pfaendtner, E. H. G. Backus, M. Bonn and T. Weidner, *J. Am. Chem. Soc.*, 2016, **138**, 5226-5229.
3. H.-K. Nienhuys and M. Bonn, *J. Phys. Chem. B*, 2009, **113**, 7564-7573.
4. L. Martinez, R. Andrade, E. G. Birgin and J. M. Martinez, *Journal of Computational Chemistry*, 2009, **30**, 2157-2164.
5. K. Lindorff-Larsen, S. Piana, K. Palmo, P. Maragakis, J. L. Klepeis, R. O. Dror and D. E. Shaw, *Proteins-Structure Function and Bioinformatics*, 2010, **78**, 1950-1958.
6. H. Lutz, V. Jaeger, R. Berger, M. Bonn, J. Pfaendtner and T. Weidner, *Advanced Materials Interfaces*, 2015, **2**, n/a-n/a.
7. D. A. Case, V. Babin, J. T. Berryman, B. R.M., Q. Cai, D. S. Cerutti, T. E. I. Cheatham, T. A. Darden, R. E. Duke, H. Gohlke, A. W. Goetz, S. Gusarov, N. Homeyer, P. Janowski, J. Kaus, I. Kolossváry, A. Kovalenko, T. S. Lee, S. LeGrand, T. Luchko, R. Luo, B. Madej, K. M. Merz, F. Paesani, D. R. Roe, A. Roitberg, C. Sagui, R. Salomon-Ferrer, G. Seabra, C. L. Simmerling, W. Smith, J. Swails, R. C. Walker, J. Wang, R. M. Wolf, X. Wu and P. A. Kollman, *AMBER 14*, University of California, San Francisco, 2014.
8. A. Sousa da Silva and W. Vranken, *BMC Research Notes*, 2012, **5**, 367.
9. B. Hess, C. Kutzner, D. van der Spoel and E. Lindahl, *Journal of Chemical Theory and Computation*, 2008, **4**, 435-447.
10. T. Darden, D. York and L. Pedersen, *Journal of Chemical Physics*, 1993, **98**, 10089-10092.
11. G. Bussi, D. Donadio and M. Parrinello, *Journal of Chemical Physics*, 2007, **126**.
12. C.-S. Hsieh, R. K. Campen, A. C. Vila Verde, P. Bolhuis, H.-K. Nienhuys and M. Bonn, *Phys. Rev. Lett.*, 2011, **107**, 116102.
13. W. Humphrey, A. Dalke and K. Schulten, *J. Mol. Graphics*, 1996, **14**, 33-38.
14. A. Savitzky and M. J. E. Golay, *Anal. Chem.*, 1964, **36**, 1627-1639.